Structural Studies of the Interactions of Normal and Abnormal Human Plasmins with Bovine Basic Pancreatic Trypsin Inhibitor

Mayuko TAKEDA-SHITAKA,*[,a] Kenshu KAMIYA,[b] Toshiyuki MIYATA,[c] Naoki OHKURA,[c] Seiji MADOIWA,[d] Yoichi SAKATA,[d] and Hideaki UMEYAMA[a]

School of Pharmaceutical Sciences, Kitasato University,[a] 5–9–1 Shirokane, Minato-ku, Tokyo 108–8641, Japan, School of Science, Kitasato University,[b] 1–15–1 Kitasato, Sagamihara, Kanagawa 228–8555, Japan, National Cardiovascular Center Research Institute,[c] Fujishirodai 5, Suita 565–8565, Japan, and Division of Thrombosis and Hemostasis, Institute of Hematology, Jichi Medical School,[d] Yakushiji, Tochigi 329–0431, Japan.
Received September 18, 1998; accepted December 14, 1998

Catalytic activity of human plasmin is inhibited by bovine basic pancreatic trypsin inhibitor (BPTI, also known as aprotinin). In spite of increased interest in the function of BPTI as an inhibitor of plasmin, the 3-D structure of the plasmin-BPTI complex has not yet been determined. Therefore, in the present paper, the structure of the plasmin-BPTI complex was constructed by the homology modeling method, which provided information about the high affinity of plasmin for BPTI. Moreover, normal mode analyses of free plasmin, free BPTI and the plasmin-BPTI complex were carried out to investigate the changes in dynamics following complex formation.

After study of the plasmin-BPTI interaction, we also investigated the binding of BPTI with abnormal plasmin, theoretically and experimentally. The result showing that BPTI binds to abnormal plasmin in the same way as it does to normal plasmin supports the previous finding that the difference between normal and abnormal plasmins is very small and that the abnormality is localized to the catalytic site.

Key words plasmin; bovine basic pancreatic trypsin inhibitor (BPTI); homology modeling; normal mode analysis

Human plasminogen is a single-chain glycoprotein that is converted by plasminogen activators to an active two-chain form, protease, human plasmin (HUPL). The heavy chain is composed of five kringle domains and the light chain is a trypsin-like serine protease domain. HUPL has various properties, the most major of which is the degradation of fibrin clots and fibrinogen (fibrinolysis). Fibrinolysis is very important in clinical therapeutics, because plasminogen activators and inhibitors can be used to treat thrombosis and hemorrhages, respectively. The catalytic activity of HUPL is controlled by antiplasmins and other serine protease inhibitors. It is well known that bovine basic pancreatic trypsin inhibitor (BPTI, also known as aprotinin), a Kunitz-type serine protease inhibitor, binds to HUPL as well as to trypsin.[1—3] In general, to understand protein-inhibitor interactions, both X-ray and model structures of the complexes are very valuable. For example, the X-ray structure of bovine trypsin (BOTR)–BPTI complex[4] provided an important view of protease-inhibitor interactions and demonstrated the high affinity of BPTI for BOTR. A modeling study of the complexes of factor Xa and the first and second Kunitz domains of tissue factor pathway inhibitor (TFPI) showed the different binding ability of these two domains.[5] Unfortunately, however, the 3-D structure of the HUPL–BPTI complex has not been determined yet by X-ray analysis or modeling studies in spite of increased interest. Therefore, in the present paper, we constructed a 3-D structure of the HUPL–BPTI complex by the homology modeling method, which provided important information about the high affinity of HUPL for BPTI. Moreover, we carried out normal mode analyses of free HUPL, free BPTI and the HUPL–BPTI complex to investigate changes in dynamics following complex formation to provide a deeper understanding of complex formation.

After the study of the interaction between HUPL and BPTI molecules, we also investigated the binding of BPTI to abnormal HUPL, both theoretically and experimentally. Several types of dysplasminogenemia (plasminogen abnormality) have been reported so far. It is noteworthy that the gene frequency of dysplasminogenemia is significantly higher among Japanese[6—9] than in other populations.[7,10] The best characterized type is the reduced activity of HUPL in patients with venous thrombosis and with retinochoroidal vascular disorders, which results from replacing Ala55 (Chymotrypsinogen numbering is used in the present paper) with Thr in the serine protease domain.[9,11—17] In serine proteases, highly conserved Ala55 is located just behind the catalytic triad (His57, Asp102 and Ser195), and is thought to contribute to the active conformation of the catalytic site.[18] Our previous modeling study of A55T HUPL showed that the cause of the reduced activity is localized to the catalytic site, in which His57 Nε2 has difficulty in accepting a proton from Ser195 Oγ due to a slight change in the side chain conformation of His57.[19] According to previous theoretical results,[19] BPTI must bind to A55T HUPL as well as to normal HUPL because even a slight change in His57 conformation does not seem to have an adverse effect on binding to BPTI. Therefore, the binding of BPTI to A55T HUPL was investigated by a modeling study, normal mode analyses and also experimentally.

Experimental

Molecular Modeling The 3-D structure of the HUPL–BPTI complex was constructed using the CHIMERA modeling system.[5] In the present paper, theoretical studies of modeling and normal mode analyses were carried out for the serine protease domain of HUPL and BPTI. The X-ray structures of BPTI with serine proteases[4,20,21] demonstrated that the orientations of the BPTI molecules toward the binding site of each serine protease are very similar. It appears very likely that BPTI binds to HUPL in the same way as previously determined X-ray structures. Therefore, the X-ray structure of BOTR, which showed the highest sequence identity to HUPL (41.3%) among the serine proteases (Fig. 1A), complexed with BPTI, (Brookhaven Protein Data Bank (PDB)[22] code 2PTC; E-chain is BOTR and I-chain is BPTI) was used as the template structure for modeling. In areas where the main chain structures of the E-chain of 2PTC did not match for HUPL, the structures of other reference proteins were used: residues 19—39 (bovine chymotrypsin; PDB code 1MTN), 58—68 (human u-PA; 1LMW),

* To whom correspondence should be addressed.

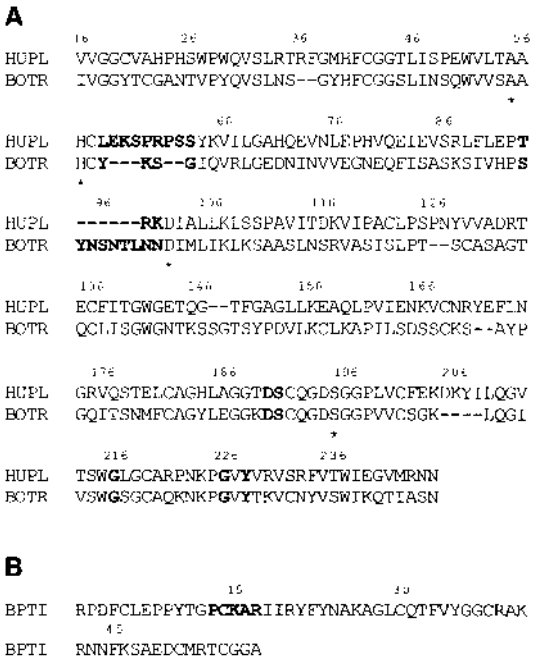

Fig. 1. Amino Acid Sequences

A: Sequence alignment of HUPL and BOTR. Chymotrypsinogen numbering is indicated above the sequences. Residues 189, 190, 216, 226 and 228 in the binding pocket, and loops 3—4 and 5—6 are indicated by bold letters. Residues with asterisks are the catalytic triad and Ala55. B: sequence of BPTI. Residues 13I—17I in the binding loop are indicated by bold letters.

70—80 (human neutrophil elastase; 1HNE), 119—138 (1MTN), 157—164 (1LMW) and 199—210 (1MTN). Two loop searches in PDB were performed at residues 92—101 and 145—152. After the main chain was constructed, the side chains were substituted to obtain the correct amino acid sequence of HUPL.

The 3-D structure of the A55T HUPL–BPTI complex was constructed based on the HUPL–BPTI complex model. Because our previous paper[19] showed that the structural differences between normal and A55T HUPLs are the side chain conformations of His57 and Asp102, the structures of residues 51—58 and 88—107, which include His57 and Asp102, respectively, were taken from a previously constructed free A55T HUPL model using CHIMERA.

The final structures derived from CHIMERA were refined by energy minimization with an AMBER united-atom force field[23] using the program APRICOT.[24] The program PROCHECK[25] was used to evaluate the stereochemical quality of the models. X-ray structures of serine protease demonstrated that there were almost no structural changes in the complex formation.[4] Also, in the case of HUPLs, it seems that no structural changes occurred, because there were no severe steric clashes between normal and A55T HUPLs and BPTI at this stage. Therefore, no further refinement using molecular dynamics was performed.

The coordinates of the models will be available at *http://prtds.pharm.kitasato-u.ac.jp/model.html*.

Normal Mode Analysis The normal mode analyses were carried out using the method described in a previous paper from our laboratory.[26] In the HUPL–BPTI complex model refined by APRICOT, there are water molecules between HUPL and BPTI in the binding pocket, because these water molecules are included in the template structure of the BOTR–BPTI complex. However, we assumed that the protein molecules were *in vacuo* in the normal mode analyses. In the present paper, we performed normal mode analyses to investigate the behavior of proteins that act like continuous elastic bodies. Such dynamic structures are mainly determined by the low-frequency modes,[27] which does not seem to be affected by the local motion of water. Therefore, the omission of water from the calculation may not be too drastic for our purposes. Instead of including the water molecules, we used a distance-dependent dielectric constant in the calculations.[28]

Firstly, we carried out the calculations of the HUPL–BPTI complex, and isolated HUPL and BPTI in their free forms. For each calculation, normal mode analyses were performed for ten structures prepared by energy minimization under different conditions. When comparing the fluctuations of isolated HUPL and BPTI with those of each corresponding part in the complex, the fluctuations must only include the internal motions. The fluctuations of the HUPL-part and BPTI-part in the complex, however, include not only internal but also external motions because the Cartesian coordinates of the complex are first defined into the coordinates of the whole complex satisfying Eckart's condition.[29] Therefore, to delete the external movements, we converted the atomic displacement of each part of the complex as the coordinates of each part satisfying Eckart's condition.[30] Secondly, we carried out the calculations on the A55T HUPL–BPTI complex, and isolated A55T HUPL and BPTI using the same methods described above.

Patient with Homozygous Plasminogen Deficiency Patient plasma showed 18% HUPL activity after activation by streptokinase when compared with normal pooled plasma. Genetic analysis was performed by the loss of a cleavage site for Fnu4HI endonuclease.[15] The patient DNA showed that a G in GCT coding for Ala55 (601, plasminogen numbering) near active site His57 (603, plasminogen numbering) was replaced by an A resulting in ACT coding for Thr as the homozygous state. The patient exhibited delayed wound healing but had no episodes of thrombosis. In this family, there was no consanguinity of the parents. Informed consent was obtained.

Preparation of Normal and Mutant Plasmin Normal and mutant plasminogen were separately purified from fresh frozen plasma or plasma of the patient, respectively, by using a lysine-immobilized column followed by an ion-exchange column and an Ultrogel ACA 44 column (IBF Biotechnics, Villeneuve-Garenne, France), as described previously.[11,12,31] Each plasminogen was activated by urokinase (Mochida Pharmaceutical Co., Tokyo) in the presence of 200 mM aminocaproic acid. Full activation was monitored by SDS-polyacrylamide gel electrophoresis under reducing conditions. BPTI was obtained from Worthington Biochemical Corp., Freehold, NJ.

Surface Plasmon Resonance Studies Binding experiments and kinetic analysis were performed using BIACORE2000 (Biacore AB, Sweden). The basic principles and its use have been documented elsewhere.[32,33] BPTI was prepared in immobilization buffer (10 mM acetate buffer, pH 5.5) to give an absorbance at 280 nm of 0.0048 and immobilized on sensor chips (CM5, certified grade, Biacore) at a flow rate of 5 μl/min at 25 °C for 60 sec by the amine coupling method.[32] The immobilization level for BPTI was 60 RUs. For binding studies, HUPL was injected over a range of concentrations between 50 nM and 800 nM at 25 °C for 180 sec at a flow rate of 10 μl/min. The sample dilution and running buffer for BIACORE2000 were both HBS (10 mM HEPES, 150 mM NaCl, 3.4 mM EDTA, and 0.005% Tween 20, pH 7.4). Prior to data collection, several methods for surface generation after ligand binding were evaluated. Injection of 100 mM HCl (5 μl) efficiently removed the bound proteins and preserved the binding capacity of the sensor chip.

The association-rate for binding between HUPL and BPTI can be expressed by the following equation[34]:

$$dR/dt = -(k_{ass}C + k_{diss})R_t + k_{ass}CR_{max}$$

where k_{ass} is the association-rate constant, k_{diss} is the dissociation-rate constant, R_{max} is the maximum binding capacity of the immobilized BPTI surface as determined by saturation with HUPL, R_t is the amount of bound HUPL measured by the surface plasmon resonance response (RU) at time t, and C is the constant concentration of HUPL injected into the BPTI surface. A linear plot of dR/dt *versus* R yields

$$\text{slope} = -(k_{ass}C + k_{diss})$$

$$\text{y intercept} = k_{ass}CR_{max}$$

dR/dt is obtained from measurements of the slope at multiple time points along the real-time association curve. By plotting the slopes of dR/dt *versus* R lines as a function of the HUPL concentration, C, a new line is obtained, and k_{ass} can be obtained as the slope. k_{diss} was determined using BIAevaluation software version 3.0 (Biacore). The affinity constant, K_D, is then calculated from k_{diss}/k_{ass}.

Results and Discussion

Interaction between HUPL and BPTI in the HUPL–BPTI Complex Model The HUPL molecule in the HUPL–BPTI complex model has two domains, each containing a six-stranded antiparallel β-sheet like other serine proteases. No unfavorable contacts between the atoms and no unnatural chiral centers are observed. In the Ramachandran plot of the main-chain ϕ–φ angles, all of the nonglycine residues are in the most favored or allowed regions. The main-chain ω

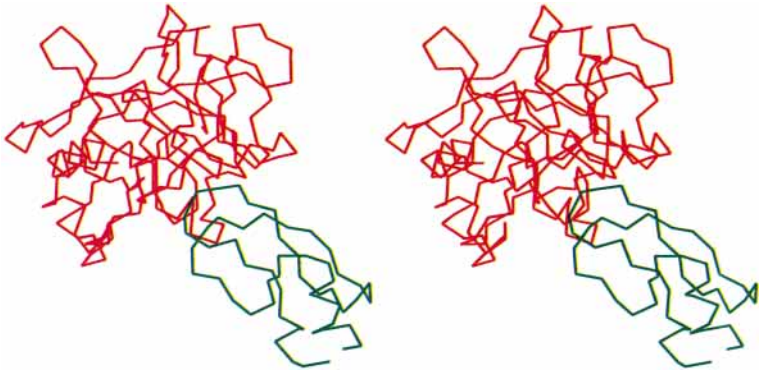

Fig. 2. Stereo View of the HUPL–BPTI Complex

View is rotated 90° along the x axis compared with the standard orientation of serine proteases shown in Figs. 3 and 5. Red, HUPL; green, BPTI.

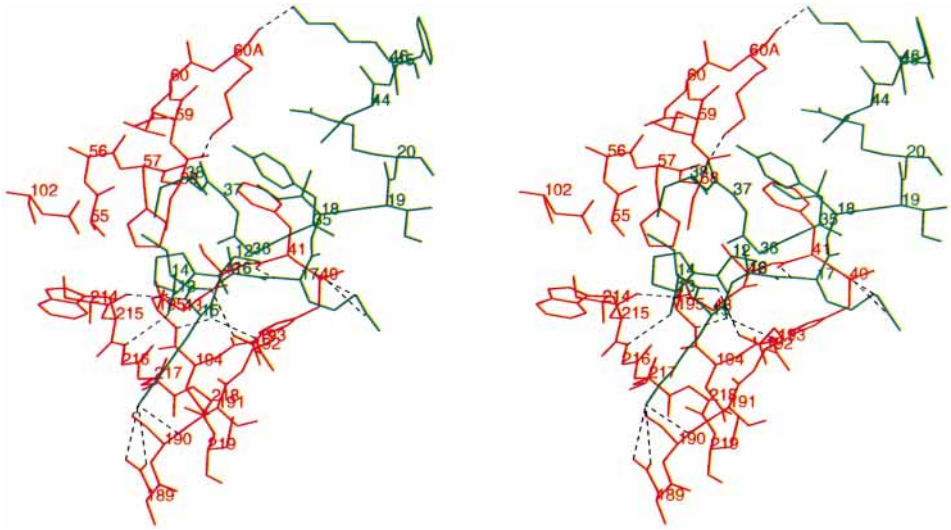

Fig. 3. Stereo View of the Intermolecular Interactions in the HUPL–BPTI Complex

Hydrogen bonds and the salt bridge listed in Table 1 are drawn with broken lines. Chymotrypsinogen numbering is indicated for HUPL. Red, HUPL; green, BPTI.

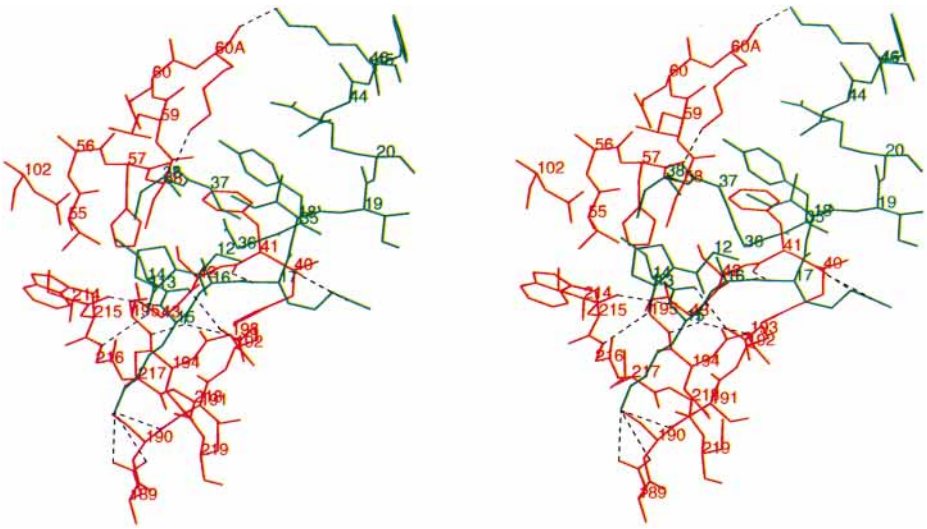

Fig. 5. Stereo View of the Intermolecular Interactions in the A55T HUPL–BPTI Complex

Hydrogen bonds and the salt bridge listed in Table 1 are drawn with broken lines. Chymotrypsinogen numbering is indicated for A55T HUPL. Red, A55T HUPL; green, BPTI.

angles are all trans-planar. The catalytic triad is in active conformation. The intermolecular orientation of HUPL and BPTI is similar to that of the X-ray structures of BPTI complexed with other serine proteases as expected (Fig. 2). An exposed binding loop (Pro13I–Ile19I, BPTI residues are distinguished by the suffix I) of BPTI fits into the active-site cleft of HUPL. There are no bad steric clashes that prevent close interaction of HUPL and BPTI.

The intermolecular interactions found in the HUPL–BPTI complex model are shown in Table 1 and Fig. 3. The primary substrate specificity among the serine proteases depends on the side chains at positions 189 (174, sequential numbering in the catalytic domain of HUPL is shown in parentheses; S1 site), 216 (201) and 226 (211) (Fig. 1A), because these residues are part of the substrate binding pocket. HUPL has Asp189 (174), Gly216 (201) and Gly226 (211), which indicates that HUPL has trypsin-like specificity toward the ligand containing Arg or Lys side chains at the P1 site. The side chains at positions 190 (175) and 228 (213) are additional determinants for substrate specificity because they are also in the substrate binding pocket.[35] HUPL has Ser190 (175) and Tyr228 (213) (Fig. 1A) which also supports the trypsin-like specificity of HUPL. In the HUPL–BPTI complex model, the side chain of Asp189 (174) at S1 and the side chain of Lys15I at P1 interact with each other through a hydrogen bond and a salt bridge, which is probably the major determinant for the high affinity of HUPL for BPTI.

Residues 13I—17I in the exposed binding loop of BPTI (Fig. 1B) form the great majority of the important contacts with the binding site of HUPL (Table 1 and Fig. 3). These primary contacts between the binding loop and the binding site are also observed in the X-ray structure of the BOTR–BPTI complex. Residues 13I—15I form an antiparallel β-sheet structure in the model, making two hydrogen bonds with the main chain of HUPL at Ser214 (199) and Gly216 (201). Residues 13I—15I also make several hydrogen bonds with residues 189—195 (174—180) of HUPL including the S1 site and the oxyanion hole. Residue 17I is hydrogen bonded to His40 (25) and Phe41 (26).

In the BOTR–BPTI complex, besides these primary contacts, there are three additional contacts outside of the binding loop of BPTI: the hydrogen bonds between Tyr39 Oη and I19I N, N97 O and R39I Nε, and N97 O and R39I Nη2. These hydrogen bonds are not found in the HUPL–BPTI complex. The first of the three is not found because HUPL has Met39 (24) instead of Tyr39. The latter two are not found because HUPL lacks residue 97 due to the shorter loop between β-strands 5 and 6 in the N-terminal domain (loop 5–6). In the case of the HUPL–BPTI complex, however, different additional contacts may be formed between HUPL and BPTI. In HUPL, although loop 5–6 is shorter, the loop between β-strands 3 and 4 in the N-terminal domain (loop 3–4) framing the active site is longer than that in BOTR (Fig. 1A). It is possible that a loop of residues 36I—45I in BPTI interacts with loop 3–4 in HUPL instead of loop 5–6. Observation of the HUPL–BPTI complex model suggested that Nζ and O atoms of Lys60A (46) in loop 3–4 are hydrogen-bonded to Gly37I O and Lys46I Nζ, respectively. However, to evaluate the formation of these additional contacts further, molecular dynamics simulations will need to be performed.

Normal Mode Analyses of Free HUPL, Free BPTI and HUPL–BPTI Complex X-ray structures of serine protease demonstrated that only very few structural changes were produced on complex formation,[4] which means that the binding of ligands to serine protease is expressed by the "lock-and-key" concept instead of the "induced-fit" concept. It is, however, generally accepted that protein molecules behave dynamically in the course of binding. For a deeper understanding of HUPL–BPTI binding, it is important to investigate the dynamics of protein molecules in both their free and complex forms. For this purpose, normal mode analysis is very useful, because it provides dynamic behavior of pico-second order for the protein molecule. Therefore, we carried out normal mode analyses of free HUPL, free BPTI and the HUPL–BPTI complex, and compared the results for a more detailed understanding of HUPL–BPTI binding.

Fluctuations of Cα atoms of free HUPL and free BPTI calculated by normal mode analyses are shown in Fig. 4. In the case of free HUPL, the fluctuations are small in the β-sheet regions and large in the loop regions. The overall structure of HUPL is probably maintained by the stability of these β-sheets. In addition to the β-sheet regions, the fluctuations of the important residues 189—195 (174—180) in the binding site, which bind to residues 13I—15I in the binding loop of BPTI (Table 1), are also small, although they are not in the β-sheet region. Because they are stabilized by hydrogen bonds in spite of being in the loop region, their fluctuations are small. Among these residues, Asp189 (174) and Asp194 (179) are smaller. The former is the substrate binding residue (S1 site) that is buried at the bottom of the specificity pocket, and the latter forms a salt bridge with the N terminal amino group creating the oxyanion hole in an enzymatically active form. The fluctuations of other residues in HUPL listed in Table 1 (His40 (25), Phe41 (26), Ser214 (199) and Gly216 (201), except Lys60A (46)) are also small because they are in the β-sheet regions. These results indicate that the binding site of HUPL as the lock is very rigid in the free form. On

Table 1. Intermolecular Interactions Observed in the HUPL–BPTI and the A55T HUPL–BPTI Complexes

Interaction partners			Distance (Å)	
BPTI[a]	–	HUPLs[b]	HUPL	A55T HUPL
Hydrogen bonds				
Pro13I O	–	Gly216 (201) N	2.99	3.09
Cys14I O	–	Gln192 (177) Nε2	2.93	2.95
Lys15I N	–	Ser214 (199) O	3.28	2.92
Lys15I Nζ	–	Asp189 (174) Oδ2	3.13	2.84
Lys15I Nζ	–	Ser190 (175) Oγ	2.94	3.03
Lys15I Nζ	–	Ser190 (175) O	2.91	2.99
Lys15I O	–	Gly193 (178) N	2.77	2.83
Lys15I O	–	Ser195 (180) N	2.96	2.90
Arg17I N	–	Phe41 (26) O	2.90	2.93
Arg17I Nε	–	His40 (25) O	3.20	2.92
Arg17I Nη2	–	His40 (25) O	2.83	2.83
Gly37I O[c]	–	Lys60A (46) Nζ[c]	2.77	2.92
Lys46I Nζ[c]	–	Lys60A (46) O[c]	3.18	2.96
Salt bridge				
Lys15I Nζ	–	Asp189 (174) Oδ1	3.76	3.58

a) Residues 13I—17I are in the binding loop, residues 37I and 46I are not. *b*) HUPLs means HUPL and A55T HUPL. Residue numbers of HUPLs are chymotrypsinogen numbering (sequential numbering in the catalytic domain of HUPLs is shown in parenthesis). *c*) There is a possibility that these two hydrogen bonds are formed outside the binding loop of BPTI.

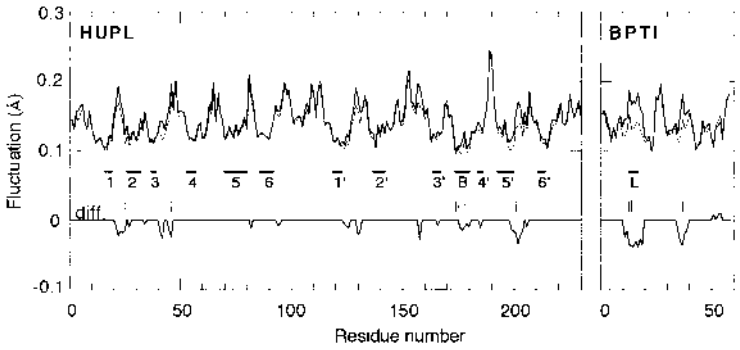

Fig. 4. Fluctuations of Cα Atoms of HUPL and BPTI

Residue numbers of HUPL represent sequential numbering of the catalytic domain of HUPL. Thick lines (free form) and thin lines (complex form): average fluctuations of the analyses of ten structures prepared by energy minimization under different conditions. Lines with 'diff.': significant difference between free and complex forms of ten structures calculated using the Wilcoxon signed rank sum test, known as a nonparametric test. Horizontal lines with numbers, which are β-sheet numbers, denote the β-sheets. Horizontal lines with 'B' and 'L' denote residues 189—195 (174—180) in the binding site of HUPL and residues 13I—17I in the binding loop of BPTI, respectively. Vertical bars denote the residues involved in the interactions listed in Table 1.

the other hand, the result of the normal mode analysis of free BPTI showed that the binding loop of BPTI as the key (residues 13I—17I) is very flexible.

Fluctuations of Cα atoms of both HUPL and BPTI in the HUPL–BPTI complex are also shown in Fig. 4. Fluctuations of some residues in the complex are smaller than those in free HUPL and free BPTI (Fig. 4). These differences are certainly caused by the complex formation, because the regions where fluctuations decrease are related to the residues forming intermolecular interactions in the HUPL–BPTI complex listed in Table 1 (also shown in Fig. 4). Firstly, we can consider the major contacts formed between the binding loop of BPTI (residues 13I—17I) and the binding site of HUPL. Before complex formation, the binding site of HUPL, as the lock, is rigid and the binding loop of BPTI, as the key, is flexible as described above, which means that the shape of the lock and the flexibility of the key play important roles when the key fits into the lock. Since the large fluctuation of the key in free form becomes considerably smaller like the β-sheet region after binding, and the small fluctuations of the lock become even smaller, it is clear that the stability of the complex is maintained by the major interactions between key and lock listed in Table 1. Secondly, we can consider the additional contacts outside the binding loop of BPTI. As listed in Table 1, two hydrogen bonds between Gly37I and Lys60A (46) and between Lys46I and Lys60A (46) are possible between HUPL and BPTI, although their formation was not evaluated by molecular dynamics simulations. The results of normal mode analyses show that fluctuations of Gly37I of BPTI and Lys60A (46) of HUPL clearly decrease following complex formation, but that of Lys46I of BPTI does not. These results mean that the additional contact between loop 3–4 in HUPL and the loop of residues 36I—45I in BPTI, including the hydrogen bond between Gly37I and Lys60A (46), may contribute to the stability of the complex. In the case of the BOTR–BPTI complex, Arg39I instead of Gly37I of BPTI forms additional contacts with BOTR. Because a loop of residues 36I—45I, which includes residues 37I and 39I, faces HUPL or BOTR in the complex structure, this loop interacts with HUPL or BOTR and stabilizes the complex. Thirdly, the fluctuations of two loops between β-strands 1′ and 2′ and between β-strands 2′ and 3′ in the C-terminal domain of HUPL decrease, although they have no direct contact with BPTI. These loops are adjacent to the binding site and the fluctuations may become smaller under the influence of BPTI binding.

A55T HUPL–BPTI Complex In addition to the HUPL–BPTI complex model, we constructed an A55T HUPL–BPTI complex model. The A55T HUPL model was based on the results of our previous papers,[19] so that the structural difference between normal and A55T HUPLs is localized to the catalytic site. In the A55T HUPL model, an unusual hydrogen bond between Thr55 Oγ1 and His57 Nε2 slightly alters the His57 conformation, such that His57 has difficulty in accepting a proton from Ser195 as the catalytic base. Observation of the complex model revealed that there are no unfavorable steric contacts that prevent close interaction between A55T HUPL and BPTI, and that the intermolecular interactions found in the HUPL–BPTI complex are also found in the A55T HUPL–BPTI complex (Table 1 and Fig. 5). This suggests that BPTI binds to A55T HUPL in the same way as it does to normal HUPL. Moreover, normal mode analyses of free A55T HUPL, free BPTI and the A55T HUPL–BPTI complex were performed to investigate the dynamics at the interface between A55T HUPL and BPTI. As shown in Fig. 6, the trends in atomic fluctuations of the free and complex forms are quite similar to those of normal HUPL and BPTI shown in Fig. 4. Suppression of atomic fluctuations by complex formation is observed in the same regions as in the normal forms. The results of normal mode analyses, together with the observations on the A55T HUPL–BPTI complex model, strongly indicate that BPTI binds to A55T HUPL just as it does to normal HUPL.

We also tested the binding of BPTI to normal and A55T HUPLs for comparison. To determine the kinetic parameters k_{ass} and k_{diss}, we injected increasing concentrations of normal and A55T HUPL molecules (50 nM—800 nM) over immobilized BPTI on the sensor chip. Sensorgrams showed a rapid increase in resonance during injections and an extremely slow decrease in the dissociation phase (Fig. 7A and 7B). For the k_{ass} value, new lines were obtained by plotting the slopes of the *dR*/*dt versus R* lines as a function of HUPL concentration, and this allowed an accurate estimation of the association-rate constant. Using this analysis, k_{ass} values between normal HUPL and BPTI and between A55T HUPL and BPTI were estimated to be $1.41\pm0.09\times10^4\,s^{-1}\,M^{-1}$ and

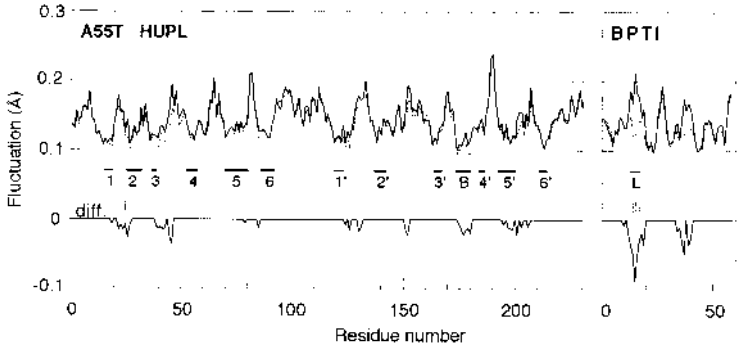

Fig. 6. Fluctuations of Cα Atoms of A55T HUPL and BPTI

Figure legend is the same as that in Fig. 4. ('HUPL' in Fig. 4 is replaced with 'A55T HUPL' in this figure.)

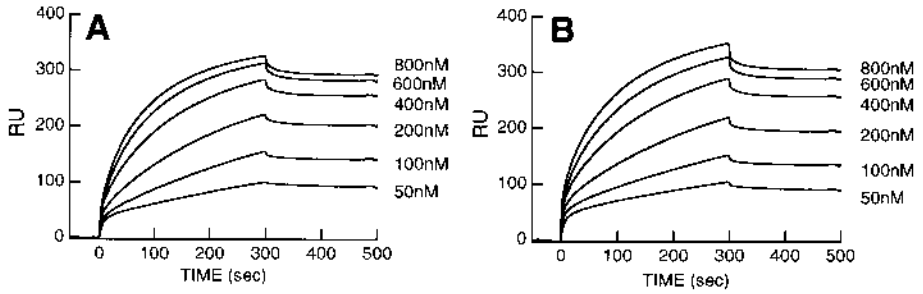

Fig. 7. Kinetic Measurements of Normal and A55T HUPLs–BPTI Interactions

Sensorgrams of the interactions with surface-bound BPTI at various concentrations (50 nM—800 nM) of normal or A55T HUPL are shown in A and B, respectively.

$0.92\pm0.16\times10^4\,s^{-1}\,M^{-1}$, respectively. The dissociation phase (325—475 s) fitted a single exponential interaction model well at concentration between 200 nM and 800 nM, and k_{diss} was calculated to be $1.45\pm0.04\times10^{-4}\,s^{-1}$ and $1.61\pm0.07\times10^{-4}\,s^{-1}$, respectively. The kinetic parameters of the binding of both normal and A55T HUPLs to BPTI are summarized in Table 2, which reveals that BPTI binds to A55T HUPL just as it does to normal HUPL. The high binding affinity of BPTI to A55T HUPL was demonstrated experimentally. This result supports the theoretical studies which showed that the structural difference between normal and A55T HUPLs is quite small and that the abnormality of the A55T HUPL molecule is localized to the catalytic site.[19] The structure of the region where the important intermolecular interactions are formed is like normal HUPL in A55T HUPL and, therefore, BPTI binds to A55T HUPL in the same way as it does to normal HUPL. BPTI (also known as aprotinin), as a protease inhibitor, has attracted attention as a treatment for pancreatitis, hemorrhage, thrombosis, malignant tumors and other conditions. The present study suggests that, when aprotinin is used in patients who have abnormal plasminogen, it may reduce the low level of activity of abnormal plasmin (18% of normal plasmin) even further.

Table 2. Kinetic Parameters Obtained from the Interaction Analysis of BPTI and HUPLs using a Biosensor

HUPLs	k_{ass} ($s^{-1}\,M^{-1}$)	k_{diss} (s^{-1})	K_D (M)
Normal	$1.41\pm0.09\times10^4$	$1.45\pm0.04\times10^{-4}$	1.03×10^{-8}
A55T	$0.92\pm0.16\times10^4$	$1.61\pm0.07\times10^{-4}$	1.75×10^{-8}

Conclusion

A modeling study of the HUPL–BPTI complex produced an important structural view of the interaction between HUPL and BPTI. HUPL has trypsin-like specificity toward ligands, which is probably the major reason for its high affinity for BPTI. In the HUPL–BPTI complex structure, many intermolecular interactions are observed. Normal mode analyses of the complex and the component molecules in their free forms revealed that suppression of the fluctuation due to complex formation is observed in regions where intermolecular interactions are formed. This indicates that these interactions make a major contribution to the stability of the complex. Moreover, the binding of BPTI to A55T HUPL was investigated both theoretically and experimentally, showing that BPTI binds to A55T HUPL in the same way as it does to normal HUPL. This result supports the conclusion of our previous paper,[19] that the abnormality of the A55T HUPL molecule is localized to the catalytic site.

Note

Quite recently, two X-ray structures of the catalytic domain of HUPL have been reported independently by two groups. One has been reported by Wang *et al*. in *Science*, published on September 11, 1998[36] and the other by Parry *et al*. in *Nature Structural Biology*, published on October 1998.[37] Although the coordinates have been deposited in PDB (PDB code of the former is 1BML, and the latter 1BUI), they are on hold until July 24 and September 4, 1999, respectively. The structural data described in the two papers are in good agreement with our model. Our previous[19] and present modeling studies showed that loop 5–6 in HUPL is relatively small compared with other serine proteases (see Fig. 3 in reference 19), and this structural feature was also described in their papers. Accordingly, this suggests that our

HUPL model for the catalytic domain is reliable and useful for structural studies of the HUPL–BPTI complex.

Acknowledgments We thank Dr. Youji Kurihara of Kitasato University for helpful discussions. This work was supported by a Grant-in-Aid for special project research from the Ministry of Education, Science, Sports and Culture in Japan.

References

1) Feeney R. E., Means G. E., Bigler J. C., *J. Biol. Chem*., **244**, 1957—1960 (1969).
2) Menegatti E., Guarneri M., Bolognesi M., Ascenzi P., Amiconi G., *J. Mol. Biol*., **191**, 295—297 (1986).
3) Ascenzi P., Amiconi G., Bolognesi M., Menegatti E., Guarneri M., *Biochim. Biophys. Acta*, **1040**, 134—136 (1990).
4) Marquart M., Walter J., Deisenhofer J., Bode W., Huber R., *Acta Crystallogr. B*, **39**, 480—490 (1983).
5) Yoneda T., Komooka H., Umeyama H., *J. Protein Chem*., **16**, 597—605 (1997).
6) Nishimukai H., Kera Y., Sakata K., Yamasawa K., *Vox. Sang*., **40**, 422—425 (1981).
7) Aoki N., Tateno K., Sakata Y., *Biochem. Genet*., **22**, 871—881 (1984).
8) Yamaguchi M., Doi S., Yoshimura M., *Hum. Hered*., **39**, 356—360 (1989).
9) Tsutsumi S., Saito T., Sakata T., Miyata T., Ichinose A., *Thromb. Haemostasis*, **76**, 135—138 (1996).
10) Skoda U., Klein A., Lubcke I., Mauff G., Pulverer G., *Electrophoresis*, **9**, 422—426 (1988).
11) Aoki N., Moroi M., Sakata Y., Yoshida N., Matsuda M., *J. Clin. Invest.*, **61**, 1186—1195 (1978).
12) Sakata Y., Aoki N., *J. Biol. Chem*., **255**, 5442—5447 (1980).
13) Miyata T., Iwanaga S., Sakata Y., Aoki N., *Proc. Natl. Acad. Sci. U.S.A*., **79**, 6132—6136 (1982).
14) Miyata T., Iwanaga S., Sakata Y., Aoki N., Takamatsu J., Kamiya T., *J. Biochem*. (Tokyo), **96**, 277—287 (1984).
15) Ichinose A., Espling E. S., Takamatsu J., Saito H., Shinmyozu K., Maruyama I., Petersen T. E., Davie E. W., *Proc. Natl. Acad. Sci. U.S.A*., **88**, 115—119 (1991).
16) Li L., Kikuchi S., Arinami T., Kobayashi K., Tsuchiya S., Hamaguchi H., *Clin. Genet*., **45**, 285—287 (1994).
17) Murata M., Ooe A., Izumi T., Nakagawa M., Takahashi S., Ishikawa M., Mori K., Ichinose A., *Brit. J. Haemato*., **99**, 301—303 (1997).
18) Takeda-Shitaka M., Umeyama H., *Chem. Pharm. Bull*., **46**, 1343—1348 (1998).
19) Takeda-Shitaka M., Umeyama H., *FEBS Lett*., **425**, 448—452 (1998).
20) Chen Z., Bode W., *J. Mol. Biol*., **164**, 283—311 (1983).
21) van de Locht A., Bode W., Huber R., Le Bonniec B. F., Stone S. R., Esmon T., Stubbs M. T., *EMBO J*., **16**, 2977—2984 (1997).
22) Bernstein F. C., Koetzle T. F., Williams G. J. B., Meyer E. F., Jr., Brice M. D., Rodgers J. R., Kennard O., Shimanouchi T., Tasumi M., *J. Mol. Biol.*, **112**, 535—542 (1977).
23) Weiner S. J., Kollman P. A., Case D. A., Singh U. C., Ghio C., Alagona G., Profeta S., Jr., Weiner P., *J. Am. Chem. Soc*., **106**, 765—784 (1984).
24) Yoneda S., Umeyama H., *J. Chem. Phys*., **97**, 6730—6736 (1992).
25) Laskowski R. A., McArthur M. W., Moss D. S., Thornton J. M., *J. Appl. Crystallogr.*, **26**, 283—291 (1993).
26) Sumikawa H., Suzuki H., Fukuhara K., Nakajima Y., Kamiya K., Umeyama H., *Chem. Pharm. Bull*., **46**, 1069—1077 (1998).
27) Go N., Noguti T., Nishikawa T., *Proc. Natl. Acad. Sci. U.S.A*., **80**, 3696—3700 (1983).
28) Thomas A., Martin J. F., Mouawad L., Perahia D., *J. Mol. Biol*., **257**, 1070—1087 (1996).
29) Eckart C., *Phys. Rev*., **47**, 552—558 (1935).
30) Ishida H., Jochi Y., Kidera A., *Proteins*, **32**, 324—333 (1998).
31) Lijnen H. R., Van Hoef B., Collen D., *Eur. J. Biochem*., **120**, 149—154 (1981).
32) Johnsson B., Lofas S., Lindquist G., *Anal. Biochem.*, **198**, 268—277 (1991).
33) Karlsson R., Roos H., Fagerstam L., Persson B., *Methods* (Orlando), **6**, 99—110 (1994).
34) Fagerstam L. G., Karlsson A. F., Karlsson R., Persson B., Ronnberg I., *J. Chromatogr*., **597**, 397—410 (1992).
35) Matsuzaki T., Sasaki C., Umeyama H., *J. Biochem*., **103**, 537—543 (1988).
36) Wang X., Lin X., Loy J. A., Tang J., Zhang X. C., *Science*, **281**, 1662—1665 (1998).
37) Parry M. A. A., Fernandez-Catalan C., Bergner A., Huber R., Hopfner K.-P., Schlott B., Guhrs K.-H., Bode W., *Nature Struct. Biol*., **5**, 917—923 (1998).